Arterial wave dynamics preservation upon orthostatic stress: a modelling perspective

Arterial wave dynamics preservation upon orthostatic stress: a modelling perspective

SUPPLEMENTARY MATERIAL

Matteo Fois[a,*], Luca Ridolfi[b], Stefania Scarsoglio[a]

[a]*Department of Mechanical and Aerospace Engineering, Politecnico di Torino, Corso Duca degli Abruzzi 24, Turin (10129), Italy*

[b]*Department of Environmental, Land and Infrastructure Engineering, Politecnico di Torino, Corso Duca degli Abruzzi 24, Turin (10129), Italy*

SM1. The 1D Arterial Model

Blood motion through 1D systemic arteries (main manuscript, Figure 1a) is governed by the following axisymmetric form of the Navier-Stokes equations for mass and momentum balance:

$$\frac{\partial A}{\partial t}+\frac{\partial Q}{\partial x}=0\,, \tag{S1}$$

$$\frac{\partial Q}{\partial t}+\frac{\partial}{\partial x}\left(\beta\frac{Q^2}{A}\right)+\frac{A}{\rho}\frac{\partial P}{\partial x}+N_4\frac{Q}{A}+Ag\sin\gamma\sin\alpha=0\,, \tag{S2}$$

where $A=A(x,t)$, $Q=Q(x,t)$ and $P=P(x,t)$ denote vessels cross-section area, blood flow rate, and blood pressure, respectively; t is time and x is the vessel axial coordinate (the detailed derivation of equations (S1)-(S2) can be found in [1] and [2]). Blood is modelled as Newtonian with constant density $\rho=1050$ Kg/m^3 and dynamic viscosity $\mu=0.004$ Pa s. Parameters β and N_4 are the Coriolis and the viscous coefficients, both obtained by assuming a flat-parabolic velocity profile over each vessel cross-section area. The term $g\sin\gamma\sin\alpha$ is introduced to account for the gravity influence onto momentum balance, where $g=9.81$ m/s is gravity acceleration, γ is the relative orientation of the single arterial vessel with respect to the frontal transverse body axis, whereas α accounts for the mutual orientation of the longitudinal body axis and the horizontal reference (*i.e.*, the tilt angle).

The tube-law assumed to close the system of equations (S1)-(S2) relates blood pressure P and vessels cross-section area A through a non-linear relationship accounting for arterial walls visco-elastic

*Corresponding author

behaviour. The adopted $P-A$ relationship reads

$$P = B_1 + B_2 A + B_3 A^2 + B_4 A^3 - B_5 \frac{1}{\sqrt{A}} \frac{\partial Q}{\partial x}, \tag{S3}$$

where coefficients $B_i = B_i(x)$ $(i = 1 \dots 5)$ are computed according to vessels visco-elastic mechanical properties as

$$B_1 = -\frac{1}{a_3^3}\left(a_5^3 + c_0^6\rho^3 + 3c_0^4\rho^2 a_5 + 3a_5^2 c_0^2 \rho\right),$$

$$B_2 = \frac{3\rho c_0^2}{A_0 a_3^3}\left(\rho^2 c_0^4 + 2\rho a_5 c_0^2 + a_5^2\right),$$

$$B_3 = -\frac{3\rho^2 c_0^4}{A_0^2 a_3^3}\left(a_5 + \rho c_0^2\right), \quad B_4 = \left(\frac{\rho c_0^2}{a_3 A_0}\right)^3, \quad B_5 = \frac{K_v h_w}{2\sqrt{A_0} r_0},$$

where $a_3 = 1914$ N$^{2/3}$/m$^{4/3}$, $a_5 = -45348$ N/m^2, K_v is the effective viscosity of the wall, h_w is the wall thickness, while A_0 and r_0 are the vessels initial (supine) cross-section area and radious, respectively (detailed derivation of equations (S3) and of coefficients B_i can be found in [1]). Coefficients B_i are expressed as functions of the local initial (supine) wave speed (c_0). The latter is a local haemodynamic parameter related to vessels wall mechanical properties. It rises with stiffer walls and with reduced lumen diameters, and it is estimated as $c_0 = a_2/(2r_0)^{b_2}$ [1], where $a_2 = 13.3$ m$^{1.3}$/s and $b_2 = 0.3$, An additional partial-collapse hyperbolic model [3] is enclosed into eq. (S3) for carotid and vertebral arteries (vessels numbered #6, 12, 13, 16, 17, 20) to deal with very low transmural pressures encountered during highly stressing conditions at upright posture and potentially leading to vessels lumen collapse [4].

Mass and total pressure conservation are imposed at arterial bifurcations (boundary conditions), while specific coupling conditions apply at the aortic entrance (through a model of the aortic valve) as well as at each distal 1D outlet branch (arteriolar and coronary microvascular junctions). Specific compatibility conditions are derived at each boundary through the method of characteristics [1, 2]. All arterial network geometrical features (vessel radii, lengths, wall thicknesses, orientations γ) and parameters (K_v) referred to a healthy, young man aged 20-30 yo (height 160 ÷ 200 cm, weigth 50 ÷ 100 kg) are reported in our previous work [2].

The lumped parameterizations of the systemic microvasculature and venous return account for blood inertia (L), the hydraulic resistance of vessels (R), and their elastic/compliant behaviour (C). The effect of gravity is reproduced by means of lumped hydrostatic pressure sources (Δp^h) placed within the longest venous and venae cavae compartments, as functions of the tilt angle α according to Stevino's law. The 0G governing equations for compartmental blood volume V, flow rate Q and consitutive pressure (p)-volume

law for the generic compartment j (with $j-1$ and $j+1$ the preceeding and following compartments, respectively) read:

$$\frac{dV_j}{dt} = Q_{j-1} - Q_j\,, \tag{S4}$$

$$\frac{dQ_j}{dt} = \begin{cases} \dfrac{p_j + \Delta p_j^h - R_j Q_j - p_{j+1}}{L_j}, \text{ if } j \in \{v, svc, ivc, avc\} \\ \dfrac{p_j - R_j Q_j - p_{j+1}}{L_j}, \text{ if } j \in \{art, cap, ven\} \end{cases}\,, \tag{S5}$$

$$V_j = V_j^{un} + \left(p_j - p_j^{ext}\right) C_j\,, \tag{S6}$$

where p^{ext} is the generic extravascular pressure, whereas subscripts *art*, *cap*, *ven*, *v*, *svc*, *ivc* and *avc* refer to the arteriolar, capillary, venular, venous and superior, inferior and abdominal venae cavae compartements of our model, respectively.

Heart chambers (*ch*) are represented through a time-varying elastance ($E_{ch}(t)$) model, according to

$$p_{ch} = E_{ch}\left(V_{ch} - V_{ch}^{un}\right) + ITP\,, \tag{S7}$$

where ITP is intrathoracic pressure.

Specific extravascular pressures (p^{ext}) are introduced onto given vascular districts. The intramyocardial pressure (*IMP*) acts directly onto the coronary myocardial layers [5], influencing coronary haemodynamics by transmitting left and right ventricle intra-chamber pressure onto the coronary vasculature. The intrathoracic pressure (*ITP*) applies to the cardiac chambers and pulmonary compartments. It represents the pressure inside the thoracic cavity, and it depends on the current body posture through the tilt angle α. *ITP* varies between ∼-2.9 mmHg at supine and ∼-6.5 mmHg at standing posture, due to the downward movement of the diaphragm when assuming the upright position, according to the following relationship [4]

$$ITP = -4.014 + 1.127\frac{g}{g_0} + 0.895\left(\frac{g}{g_0}\right)^2 \sin(\alpha) - 4.508\frac{g}{g_0}\sin(\alpha)\,, \tag{S8}$$

where g is the current gravity acceleration value while $g_0 = 9.81$ m/s^2 and α is the tilt angle. Finally, the intracranial pressure (*ICP*) is the cerebrospinal fluid pressure, a fluid media surrounding the brain and contained within the spinal cord. *ICP* acts onto the cerebral venous compartment, and it changes with body position from ∼10 mmHg at supine to ∼-2.8 mmHg at standing posture because of downward shifting of the cerebrospinal fluid when assuming the upright position [2, 4].

The short-term regulation included to pursue the CVS homeostasis accounts for (i) a baroreflex model to control arterial aortic-carotid sinus pressure by regulating cardiac chronotropic and inotropic

behaviour, peripheral vasodilation/constriction and venous tone; (ii) a cardio-pulmonary reflex model to control the central venous pressure (in turn by regulating peripheral resistance and venous tone); and (iii) a cerebral autoregulation model to preserve the cerebral blood flow during posture changes by modulating cerebral arteriolar resistance and compliance. Baroreflex and cardiopulmonary reflex control the CVS response according to the following model equation [2]:

$$\frac{dy}{dt} = \frac{1}{\tau}\Big(-y + \alpha\, n_s - \beta\, n_p + \gamma \Big), \tag{S9}$$

where α, β, γ and τ are saturation and delay of response parameters associated with the control of variable y (*i.e.*, HR, peripheral resistance, heart elastances, venous volumes and compliances). Parameters n_s and n_p denote sympathetic and parasympathetic activities, determined upon given target arterial and venous pressure levels. The cerebral autoregulation instead controls cerebral arteriolar compliances and resistances according to a sigmoidal function and to Poiseuille's law, respectively, targeting a given reference value of cerebral blood flow [2].

1D governing equations are discretized in space according to a Discontinuous Galerkin approach, and integrated in time via a 2-step Runge-Kutta algorithm together with 0D compartments and short-term controls ordinary differential equations.

Graded HUT from the supine (0°) to upright standing (90°) postures is performed as described in [2].

SM2. Wave Separation and WIA

Considering the pressure P and flow Q signals taken at a given point of the arterial network, they can be expressed as the summation of their respective forward (subscript f) and backward (subscript b) travelling components as

$$P = P_f + P_b\,, \tag{S10}$$

$$Q = Q_f + Q_b\,. \tag{S11}$$

From the water-hammer equation [6] it follows that $P_{f,b} = \pm Z_c Q_{f,b}$ (taking the sign '$+$' for foward waves with subscript f, whereas the sign '$-$' for backward waves with subscript b), where Z_c is the local vessel characteristic impedance. Therefore, the forward and backward components of P and Q signals can be expressed as

$$P_{f,b} = \frac{P \pm Z_c Q}{2}, \tag{S12}$$

$$Q_{f,b} = \frac{Q \pm P/Z_c}{2}. \tag{S13}$$

Wave intensity (WI) is defined as the power per unit vessel area carried by successive 'wavefronts' (infinitesimal waves) dP, dU and dQ which cumulatively form the original time signals P, U and Q, respectively, that is

$$WI = dP\,dU\,. \tag{S14}$$

Usually, a different version of equation (S14) is used to avoid the sampling frequency dependence of dP and dU, by taking their temporal normalization [6]:

$$WI = \frac{dP}{dt}\frac{dU}{dt}\,. \tag{S15}$$

WI can be separated into its forward (WI_f) and backward (WI_b) components, expressed as

$$WI_{f,b} = \frac{dP_{f,b}}{dt}\frac{dU_{f,b}}{dt}\,. \tag{S16}$$

Then, by applying equations (S12)-(S13) (with $U = Q/A$) to (S16), the following equations for forward and backward wave intensity are obtained:

$$WI_{f,b} = \pm\frac{1}{4\rho c}\left(\frac{dP}{dt} \pm \rho c\frac{dU}{dt}\right)^2, \tag{S17}$$

taking the sign '$+$' for foward WI with subscript f, wheres the sign '$-$' for backward WI with subscript b, and where the local wave speed c is computed according to the PU-loop method. The original P and U signals are pre-processed by applying a moving average filter aimed at smoothing spurious numerical oscillations.

SM3. Supplementary Tables

At the ascending aorta (site #63), the first forward WI peak (*i.e.*, the first forward compression wave, FCW) is almost identical between supine and standing position (12.7 MW/m^2/s^2 vs. 12.3 MW/m^2/s^2, respectively), despite the strong contraction of aortic forward pulse pressure (-10% from supine to standing at site #63) which should cause the first WI peak to reduce markedly from supine to standing. Several authors [6–8] have proposed a correlation between the first FCW peak of WI and the maximum slope of the left ventricle pressure waveform - $(dP/dt)_{lv,max}$ or $(dP/dt)^2_{lv,max}/(\rho c)$ - which is considered as the main (external) cause for the first forward compression impulse transmitted throughout the aorta. In Supplementary Table 1 we reported the results for these two parameters adopted as proxies of left ventricular activity, at supine and standing postures. As we can see by comparing data in Supplementary Table 1 and the first supine and standing FCW peaks of the ascending aorta WI (Figure 4, main manuscript), the

Supplementary Table 1: Left ventricular activity in terms of maximum left ventricle pressure waveform slope, according to [6–8].

Parameter	supine	standing	Δ%
$\left(dP/dt\right)_{lv,max}$ [mmHg/s]	1420	1540	+8.4%
$\left(dP/dt\right)^2_{lv,max}/(\rho c)$ [mmHg^2 m^2/(kg s)]	526	557	+5.9%

Supplementary Table 2: Standing vs. supine wave velocity (c) computed along the arterial tree at sites specified by the numbers in the left column (refer to Figure 1, main manuscript). c values are reported as mean $\pm$ standard deviation computed over the segments composing each vessel, according to the procedure illustrated in Figure 2, main manuscript (p-values are computed via Wilcoxon non-parametric test for paired samples, Δ% indicates the percentage difference between standing and supine values).

Vessel	c [m/s]			
Aorta	supine	standing	Δ%	p-value
Root #1	3.97 ± 0.02	4.19 ± 0.09	+5.4%	0.500
Ascending #63	3.89 ± 0.14	4.10 ± 0.14	+5.3%	0.031
Arch #2	4.12 ± 0.04	4.29 ± 0.03	+4.0%	0.125
Arch #14	4.24 ± 0.22	4.45 ± 0.22	+5.0%	0.008
Thoracic #18	4.32 ± 0.14	4.59 ± 0.11	+6.1%	0.002
Thoracic #27	4.65 ± 0.11	5.17 ± 0.15	+11.3%	0.002
Abdominal #28	4.74 ± 0.22	5.39 ± 0.27	+13.7%	0.002
Abdominal #35	4.86 ± 0.17	5.54 ± 0.27	+14.0%	0.125
Abdominal #37	4.85 ± 0.15	5.64 ± 0.15	+16.4%	0.125
Abdominal #39	5.00 ± 0.10	6.04 ± 0.11	+20.8%	0.002
Iliac bif. #41	5.06 ± 0.07	6.32 ± 0.09	+24.9%	0.125
Carotid				
Common carotid #5	5.43 ± 0.16	5.42 ± 0.11	-0.1%	0.770
External carotid #13	6.77 ± 0.15	6.55 ± 0.12	-3.2%	0.031
Brachial				
Subclavian/brachial #21	6.03 ± 0.15	6.74 ± 0.50	+11.9%	0.002
Ulnar #23	7.03 ± 0.25	8.44 ± 0.29	+20.1%	0.002
Interosseous #24	9.01 ± 0.49	10.73 ± 0.97	+19.1%	0.002
Legs				
Common iliac #42	5.75 ± 0.09	7.16 ± 0.11	+24.5%	0.002
External iliac #44	6.16 ± 0.06	7.74 ± 0.12	+25.6%	0.002
Femoral #46	6.71 ± 0.15	8.91 ± 0.38	+32.8%	0.002
Tibial #48	7.42 ± 0.11	10.78 ± 0.38	+45.2%	0.002

Supplementary Table 3: Standing vs. supine forward pulse pressure (PP_f), backward pulse pressure (PP_b), reflection magnitude (RM) and reflection index (RI) computed along the arterial tree at sites specified by the numbers in the left column (refer to Figure 1, main manuscript). PP_f and PP_b mean $\pm$ standard deviation values over each vessel are reported - computed as illustrated in Figure 2, main manuscript ($\Delta\%$ indicates the percentage difference between standing and supine values).

Vessel	PP_f [mmHg]			PP_b [mmHg]			RM			RI		
Aorta	supine	standing	$\Delta\%$	supine	standing	$\Delta\%$	supine	standing	$\Delta\%$	supine	standing	$\Delta\%$
#1	40 ± 0.22	37 ± 0.10	-9.9%	22 ± 0.04	18 ± 0.02	-17.3%	0.54	0.49	-8.2%	0.35	0.33	-5.5%
#63	41 ± 0.25	37 ± 0.19	-10.4%	22 ± 0.11	18 ± 0.05	-17.1%	0.53	0.49	-7.5%	0.35	0.33	-5.0%
#2	47 ± 0.49	41 ± 0.38	-11.9%	20 ± 0.06	16 ± 0.03	-16.1%	0.42	0.40	-4.9%	0.30	0.29	-3.5%
#14	51 ± 0.11	45 ± 0.12	-12.0%	19 ± 0.14	16 ± 0.16	-15.7%	0.38	0.36	-4.2%	0.27	0.26	-3.1%
#18	53 ± 0.49	47 ± 0.49	-11.9%	19 ± 0.10	16 ± 0.09	-14.8%	0.35	0.34	-3.4%	0.26	0.25	-2.5%
#27	62 ± 2.35	55 ± 2.44	-11.3%	19 ± 1.51	17 ± 1.65	-9.1%	0.31	0.31	+2.4%	0.23	0.24	+1.9%
#28	65 ± 1.66	59 ± 1.82	-9.7%	27 ± 1.52	25 ± 1.91	-8.9%	0.42	0.42	+0.9%	0.29	0.30	+0.6%
#35	62 ± 1.11	56 ± 1.11	-9.8%	25 ± 0.85	22 ± 0.95	-10.4%	0.40	0.39	-0.6%	0.28	0.28	-0.4%
#37	60 ± 0.87	54 ± 0.70	-9.6%	23 ± 0.66	21 ± 0.59	-9.3%	0.39	0.39	+0.3%	0.28	0.28	+0.2%
#39	60 ± 0.24	54 ± 0.26	-8.7%	25 ± 0.39	23 ± 0.33	-8.4%	0.41	0.42	+0.4%	0.29	0.29	+0.3%
#41	62 ± 0.23	57 ± 0.28	-8.7%	25 ± 0.09	23 ± 0.03	-8.3%	0.41	0.41	+0.5%	0.29	0.29	+0.4%
Carotid												
#5	46 ± 6.32	43 ± 6.03	-7.1%	27 ± 0.82	23 ± 2.51	-17.1%	0.54	0.53	-10.8%	0.37	0.35	-7.0%
#13	61 ± 1.58	57 ± 1.30	-6.3%	24 ± 0.21	17 ± 0.25	-31%	0.40	0.29	-26.4%	0.28	0.23	-20.5%
Brachial												
#21	65 ± 8.86	59 ± 8.59	-9.9%	25 ± 2.18	22 ± 2.56	-11.5%	0.38	0.38	-1.8%	0.28	0.27	-1.3%
#23	82 ± 2.48	76 ± 1.86	-7.0%	25 ± 0.84	22 ± 0.67	-14.8%	0.31	0.29	-8.4%	0.24	0.22	-6.5%
#24	72 ± 3.27	69 ± 4.15	-3.8%	36 ± 0.38	32 ± 0.76	-8.7%	0.50	0.47	-5.1%	0.33	0.32	-3.5%
Legs												
#42	65 ± 1.56	59 ± 1.46	-8.1%	25 ± 0.07	23 ± 0.22	-8.0%	0.39	0.39	+0.1%	0.28	0.28	+0.1%
#44	70 ± 0.31	64 ± 0.70	-8.1%	29 ± 0.89	26 ± 0.56	-9.1%	0.42	0.41	-1.0%	0.29	0.29	-0.7%
#46	76 ± 4.20	74 ± 5.55	-2.1%	38 ± 1.32	33 ± 0.57	-13.5%	0.51	0.45	-11.7%	0.34	0.31	-8.1%
#48	79 ± 1.33	85 ± 0.51	+8.7%	34 ± 2.31	27 ± 3.02	-20.9%	0.44	0.32	-27.2%	0.31	0.24	-20.6%

Supplementary Table 4: Standing vs. supine area ratio (A_d/A_p) at bifurcations specified by the vessel numbers in the left column (refer to Figure 1, main manuscript). Letters d and p denote the daughters and parent vessels of a bifurcation, respectively (the total daughter area is taken as the summation of all single-daughter vessel areas).

Bifurcation	A_d/A_p			Bifurcation	A_d/A_p		
#p - d1, d2, ...	supine	standing	Δ%	#p - d1, d2, ...	supine	standing	Δ%
#1 - 49, 58, 63	1.045	1.044	-0.11%	#18 - 26, 27	1.214	1.208	-0.49%
#63 - 2, 3	1.167	1.163	-0.32%	#27 - 28, 29	1.266	1.258	-0.65%
#3 - 4, 5	1.226	1.225	-0.07%	#29 - 30, 31	1.185	1.178	-0.60%
#4 - 6, 7	1.186	1.186	+0.01%	#29 - 30, 31	1.185	1.178	-0.60%
#7 - 8, 9	1.244	1.232	-0.94%	#28 - 34, 35	1.315	1.305	-0.76%
#9 - 10, 11	1.270	1.262	-0.63%	#35 - 36, 37	1.179	1.173	-0.53%
#5 - 12, 13	1.173	1.176	+0.28%	#37 - 38, 39	1.164	1.157	-0.59%
#2 - 14, 15	1.119	1.116	-0.23%	#39 - 40, 41	1.150	1.141	-0.74%
#15 - 16, 17	1.258	1.262	+0.30%	#41 - 42, 42	1.160	1.142	-1.55%
#14 - 18, 19	1.213	1.211	-0.18%	#42 - 43, 44	1.167	1.154	-1.05%
#19 - 20, 21	1.189	1.189	-0.02%	#44 - 45, 46	1.162	1.145	-1.44%
#21 - 22, 23	1.233	1.222	-0.92%	#46 - 47, 48	1.139	1.117	-1.96%
#23 - 24, 25	1.229	1.224	-0.39%				

higher ventricular pressure slope may compensate the reduction expected for the first FCW, resulting in supine vs. standing first FCW peaks almost identical in amplitude.

Supplementary Table 2 shows supine vs. standing wave velocity c computed within several vessels of the arterial tree (p-values computed by Wilcoxon's test of significance for paired samples), while Supplementary Table 3 reports values of PP_f, PP_b, RM and RI (forward and backward pulse pressure, reflection magnitude and reflection index, respectively).

Supplementary Table 4 reports values of supine and standing daughters-to-parent (subscripts d and p, respectively) vessels area ratios A_d/A_p for every bifurcation included in the present 1D arterial network (numbers indicating vessels involved in bifurcations are reported on the left column of Supplementary Table 4, as parent - daughter 1, daughter 2, etc.), where the total cross-section area of daughter vessels A_d is taken as the summation of all single-daughter vessel areas originating from the corresponding parent vessel of the bifurcation.

SM4. Supplementary Figures

Supplementary Figure 1 shows an example of WI computation corresponding to the entrance of the aorta (vessel #1, first segment) for the supine body position. The different peaks of the forward and backward WI profiles are associated with corresponding increase or decrease of the related forward and

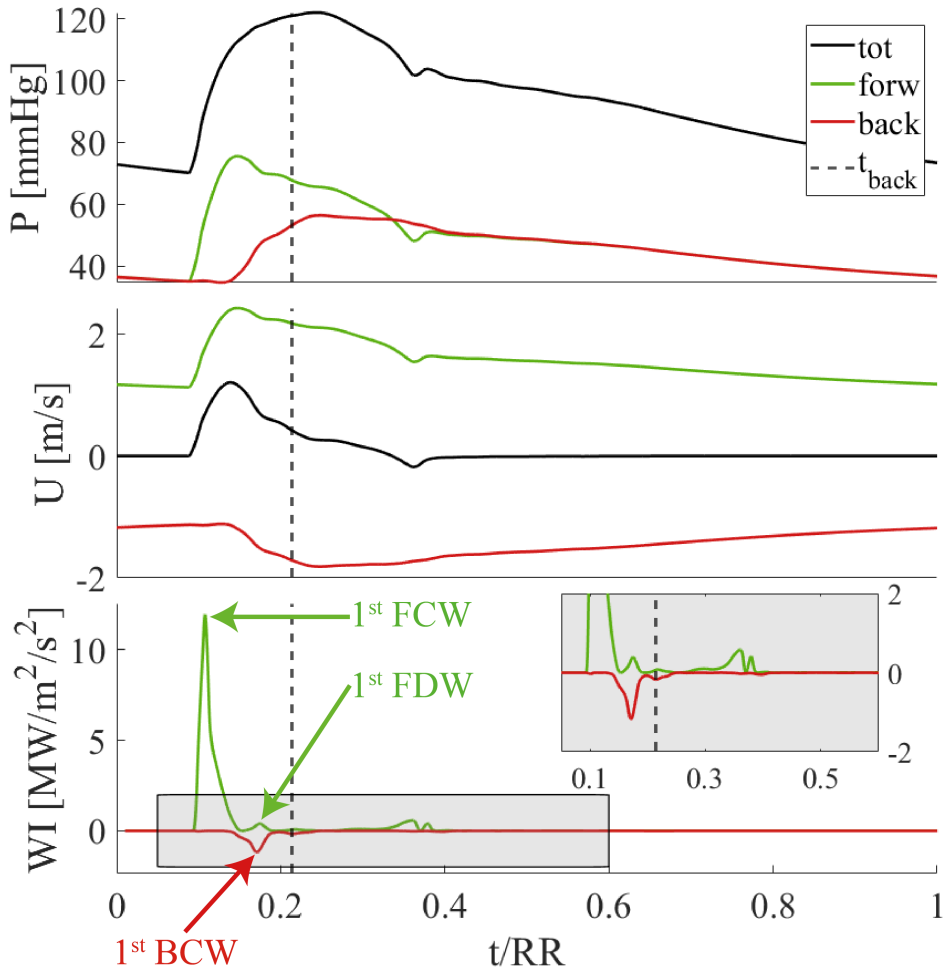

Supplementary Figure 1: In the upper and central panels the total (tot) and separated forward (forw) and backward (back) pressure P and flow velocity U signals are represented. An example of WI computation at the entrance of the aorta ($e = 1$) is shown in the lower panel (the inset displays a magnification of the gray shaded area). t_{back} is the average arrival time of backward waves; FCW, FDW and BCW indicate forward compression or decompression waves, and backward compression wave, respectively. Time t is normalized with the heartbeat duration, RR.

backward pressure signal. Typically, a forward (*i.e.*, green) WI peak is named as a forward compression wave (FCW) if it corresponds to a local increase in forward pressure signal (such as for the first, strong forward WI peak, associated with the compression wave originated from upstream by the left ventricle contraction). Differently, a forward WI peak is termed as a forward decompression/expansion wave (FDW) if it corresponds to a local decrease in forward pressure signal (such as for the late-systolic expansion wave originated by the aortic valve closure, at the dicrotic notch). The same nomenclature is used for backward (*i.e.*, red) WI peaks, with the first, evident backward WI peak shown in Supplementary Figure 1 being a backward compression wave (BCW) originated by the downstream reflection of the first FCW discussed previously.

Supplementary Figure 2 displays the computed R_p at bifurcations (forward waves on top, backward waves on bottom side) for the supine and standing position.

Supplementary Figure 3 displays the computed R_p due to vessels tapering (on top) and to peripheral resistance (bottom) for the supine and standing position.

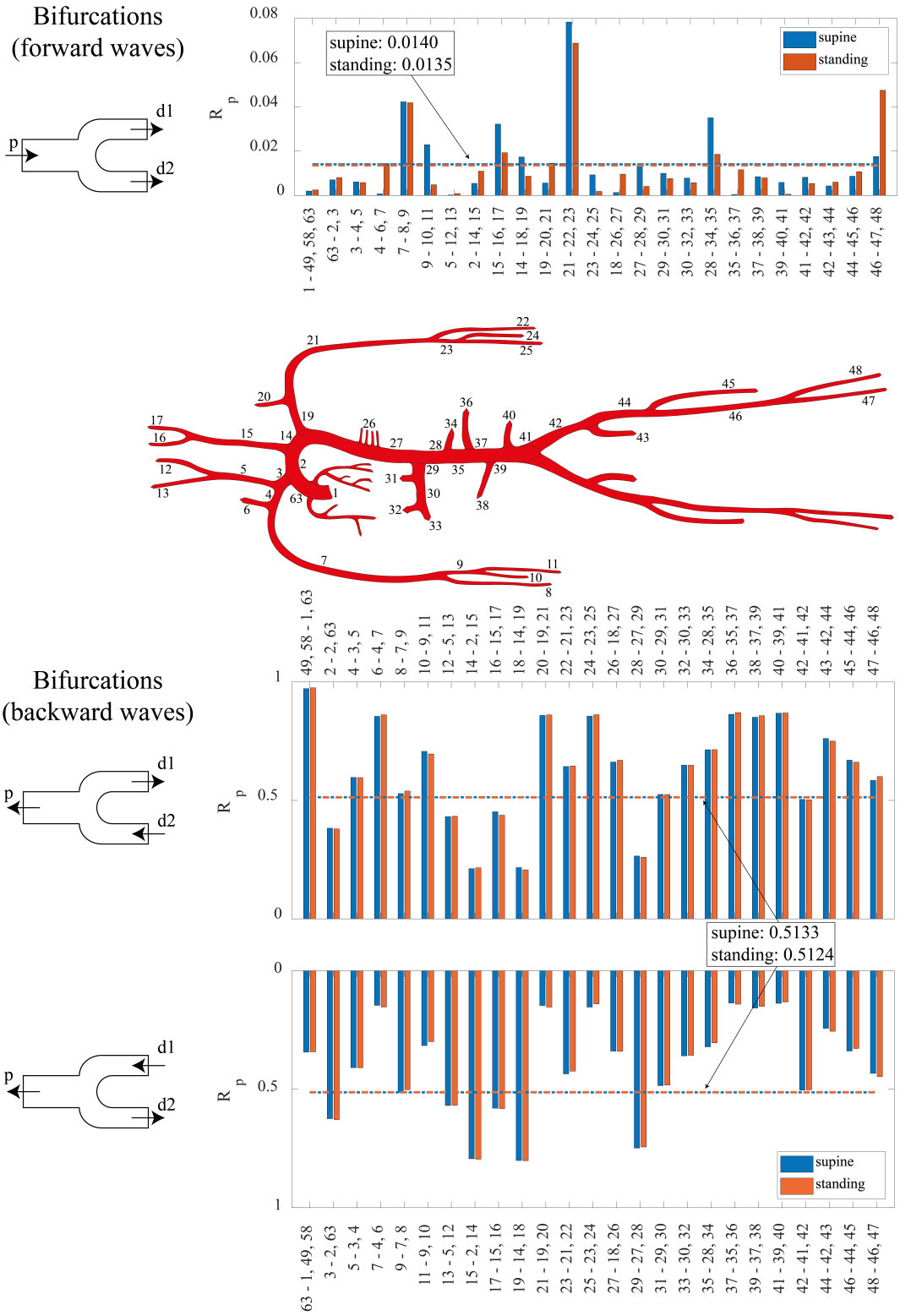

Supplementary Figure 2: Pressure reflection coefficient R_p at supine (blue bars) and standing (orange bars) postures computed at arterial bifurcations for the forward (top diagram) and backward (bottom diagrams) wave transmission case. Arterial bifurcations are identified by the involved vessels as parent vessel (p) - daughter vessel 1 (d1), daughter vessel 2 (d2), etc.

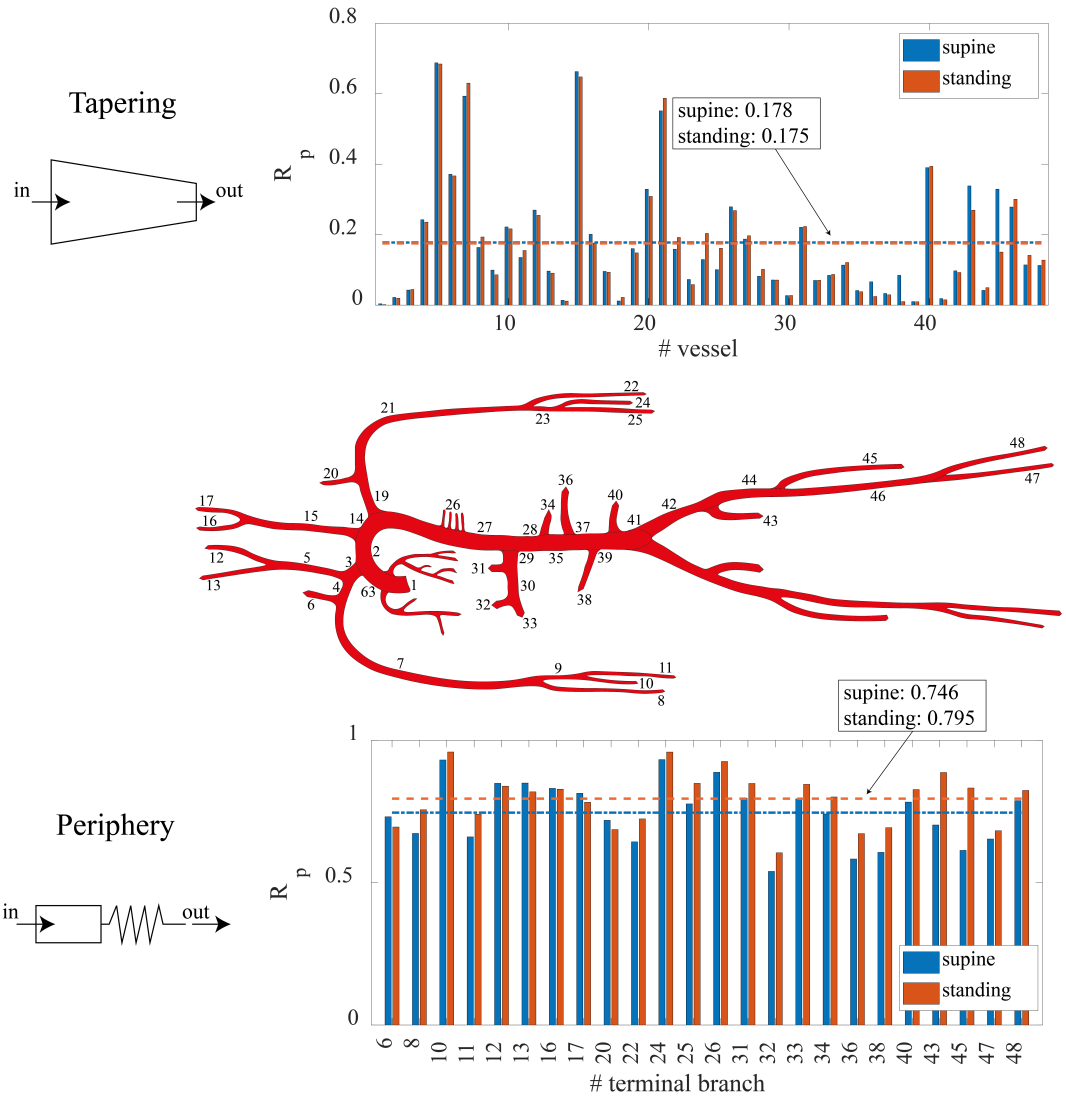

Supplementary Figure 3: Pressure reflection coefficient R_p at supine (blue bars) and standing (orange bars) postures associated with arterial vessels tapering (top diagram) and peripheral resistance (bottom diagrams). Arterial vessels are indicated by numbers with reference to Figure 1, main manuscript.

References

[1] A. Guala, C. Camporeale, F. Tosello, C. Canuto, L. Ridolfi, Modelling and subject-specific validation of the heart-arterial tree system, Annals of biomedical engineering 43 (1) (2015) 222–237. doi:10.1007/s10439-014-1163-9.

[2] M. Fois, S. V. Maule, M. Giudici, M. Valente, L. Ridolfi, S. Scarsoglio, Cardiovascular response to posture changes: Multiscale modeling and in vivo validation during head-up tilt, Frontiers in Physiology 13 (826989) (2022). doi:10.3389/fphys.2022.826989.

[3] G. Drzewiecki, S. Field, I. Moubarak, J. K.-J. Li, Vessel growth and collapsible pressure-area relationship, American Journal of Physiology-Heart and Circulatory Physiology 273 (4) (1997) H2030–H2043. doi:10.1152/ajpheart.1997.273.4.H2030.

[4] M. Fois, L. Ridolfi, S. Scarsoglio, In silico study of the posture-dependent cardiovascular performance during parabolic flights, Acta Astronautica 200 (2022) 435–447. doi:10.1016/j.actaastro.2022.08.018.

[5] A. Saglietto, M. Fois, L. Ridolfi, G. M. De Ferrari, M. Anselmino, S. Scarsoglio, A computational analysis of atrial fibrillation effects on coronary perfusion across the different myocardial layers, Scientific reports 12 (841) (2022). doi:10.1038/s41598-022-04897-6.

[6] J. P. Mynard, A. Kondiboyina, R. Kowalski, M. M. Cheung, J. J. Smolich, Measurement, analysis and interpretation of pressure/flow waves in blood vessels, Frontiers in Physiology (2020). doi:10.3389/fphys.2020.01085.

[7] N. Ohte, H. Narita, M. Sugawara, K. Niki, T. Okada, A. Harada, J. Hayano, G. Kimura, Clinical usefulness of carotid arterial wave intensity in assessing left ventricular systolic and early diastolic performance, Heart and vessels 18 (3) (2003) 107–111. doi:10.1007/s00380-003-0700-5.

[8] C. J. Jones, M. Sugawara, Y. Kondoh, K. Uchida, K. H. Parker, Compression and expansion wavefront travel in canine ascending aortic flow: wave intensity analysis, Heart and vessels 16 (3) (2002) 91–98. doi:10.1007/s003800200002.